JOURNAL OF MATERIALS SCIENCE 21 (1986) 2735–2743

A study of multiple fracture phenomenon of a coating film on a metal fibre by means of computer simulation

SHOJIRO OCHIAI, KOZO OSAMURA
Department of Metallurgy, Kyoto University, Kyoto 606, Japan

Multiple fracture phenomenon of coating film on ductile metal fibre was studied by means of a computer simulation technique. The simulation experiments were carried out for various combinations of mechanical factors such as strength of coating film, Young's and shear moduli of fibre and coating film, yield stress of fibre and strain hardening coefficient of fibre and geometrical factors such as diameter of fibre and thickness of coating film. The effects of these factors on the number of fractures of the coating film and length of segmented film as a function of applied tensile stress and elongation to failure of coated fibre were clarified.

1. Introduction

When ductile or notch-insensitive metals are coated with a film of hard material, the film often exhibits multiple fracture phenomenon under tensile loading [1–6] in the following process. As the strain to failure of coating film is, in general, lower than that of the metals, the film breaks in the early stage of deformation. The breakdown of the coating film in one cross-section causes a drop in load bearing capacity of the specimen. In this cross-section, however, the metals work-harden and the load bearing capacity of this cross-section rises again so that the film once-fractured fails again in another cross-section. With a repetition of this process, the coating film fractures continually into shorter lengths [7]. In this process, one of the most important factors is the exerted tensile stress in the segmented (discontinuous) film, since if the exerted stress is higher than the strength of a segment, the segment is broken again. In the following paper, a new approach on stress distribution in segments will be presented [8]. According to this approach, the exerted tensile stress in segments is highest at $x = l/2$ where x is the distance from the end of segments and l is the length of segments. However, this result does not necessarily mean that each segment is broken at $x = l/2$. The fracture of segments occurs at the cross-section where the exerted stress σ_2 becomes higher than the strength in a following manner. The stress distribution in a segment, σ_2, is given as a function of x, as schematically shown in Fig. 1. Noting the strength of the cross-section at $x = a_1$, a_2 and $l/2$ in Fig. 1 as $S(a_1)$, $S(a_2)$ and $S(l/2)$, respectively and the exerted stress at $x = a_1$, a_2 and $l/2$ as $\sigma_2(a_1)$, $\sigma_2(a_2)$ and $\sigma_2(l/2)$, respectively, the cross-section at $x = a_1$ will be fractured if $\sigma_2(a_1)$ becomes higher than $S(a_1)$ while $\sigma_2(a_2)$ and $\sigma_2(l/2)$ are lower than $S(a_2)$ and $S(l/2)$, respetively. This corresponds to the case where the maximum flaw exists at $x = a_1$ and the strength of the cross-section at $x = a_1$ is weakest among the cross-sections at $x = a_1$, a_2 and $l/2$. In this case, although the exerted stress $\sigma_2(a_1)$ is lower than $\sigma_2(a_2)$ and $\sigma_2(l/2)$, the $\sigma_2(a_1)$ is high enough to break the weakest cross-section at $x = a_1$ while the exerted stresses are not high enough to break the cross-sections at $x = a_2$ and $l/2$. However, even if the maximum flaw exists at $x = a_1$, the cross-section at $x = a_2$ will be fractured if $\sigma_2(a_1) < S(a_1)$, $\sigma_2(a_2) > S(a_2)$ and $\sigma_2(l/2) < S(l/2)$. This case occurs when the exerted stress is not high enough to break the cross-section with the maximum flaw but the exerted stress becomes higher than the strength of the cross-section other than that at $x = a_1$. The fracture at $x = l/2$ occurs only when σ_2 becomes higher than S at $x = l/2$ but not $x = a_1$ and a_2. Thus the mutliple-fracture of coated layer is strongly dependent on the exerted stress distribution and location of flaws in segments. The location of flaws is rather probabilistic. To treat such probabilistic phenomena, a computer simulation technique using the Monte Carlo method is useful. The aim of the present paper is to describe the multiple-fracture phenomenon of the coating film on metal fibre (or wire) by means of the computer simulation.

2. Computer simulation procedure

The computer simulation on the multiple-fracture phenomenon of the coating film on metal fibre was carried out following the flow chart shown in Fig. 2. The details of the procedure are as follows.

(a) Mechanical factors of Young's moduli of fibre E_1 and coating film E_2, shear moduli of the fibre G_1 and the film G_2, tensile σ_{1y} and shear τ_{1y} yield stresses of fibre, tensile and shear strain hardening coefficients ω and β normalized with respect to Young's and shear moduli of fibre are defined, respectively, and the geometrical factors of diameter of fibre d, thickness of coating film c and initial length of the film l_0 were input first. The strength distribution of the coating film was assumed to obey the Weibull distribution [9]. The

0022–2461/86 $03.00 + .12

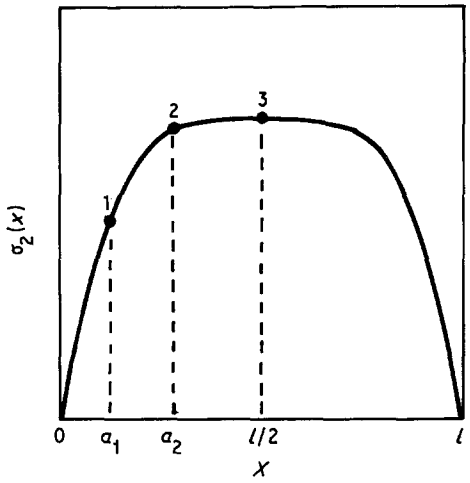

Figure 1 Schematic representation of tensile stress distribution in a segment of coating film with length l.

Weibull distribution provides the probability of P of failure at stress σ as

$$P = 1 - \exp\{-V[(\sigma - \sigma_u)/\sigma_0]^m\} \quad (1)$$

where m is the Weibull modulus, V is the volume of material, σ_0 is the normalizing factor and σ_u is the stress below which there is no probability of failure. σ_u is in general very low and is often treated as zero. In the simulation, m and σ_0 were input and σ_u was treated as zero. Various combinations of the above parameters were examined in this work. The used values of these parameters will be presented in each figure caption and in the text.

(b) The coating film with an initial length l_0 was divided into N elements with a length l_e as shown in Fig. 3a where the centres of the first and the last elements are located at the ends of the coating film. N was therefore equal to $l_0/(l_e + 1)$. In this work, l_e was taken to be 1 μm.

(c) The strength of the first and the last elements was taken to be zero. The strength of other elements was determined using the Monte Carlo method assuming that the strength of coating film is described by the Weibull distribution [9], as already stated. By substituting m and σ_0 into Equation 1 and the volume of the element $V = \{\pi[(d + 2c)^2 - d^2]l_e/4\}$ into Equation 1 strength values were generated. The generated values were distributed in the elements except the first and the last ones. Thus the strength of the ith (for $i = 2$ to $N - 1$) element, $S(i)$, was determined.

(d) Given the applied tensile stress σ_c on the composite (the coated fibre is regarded as a composite), the

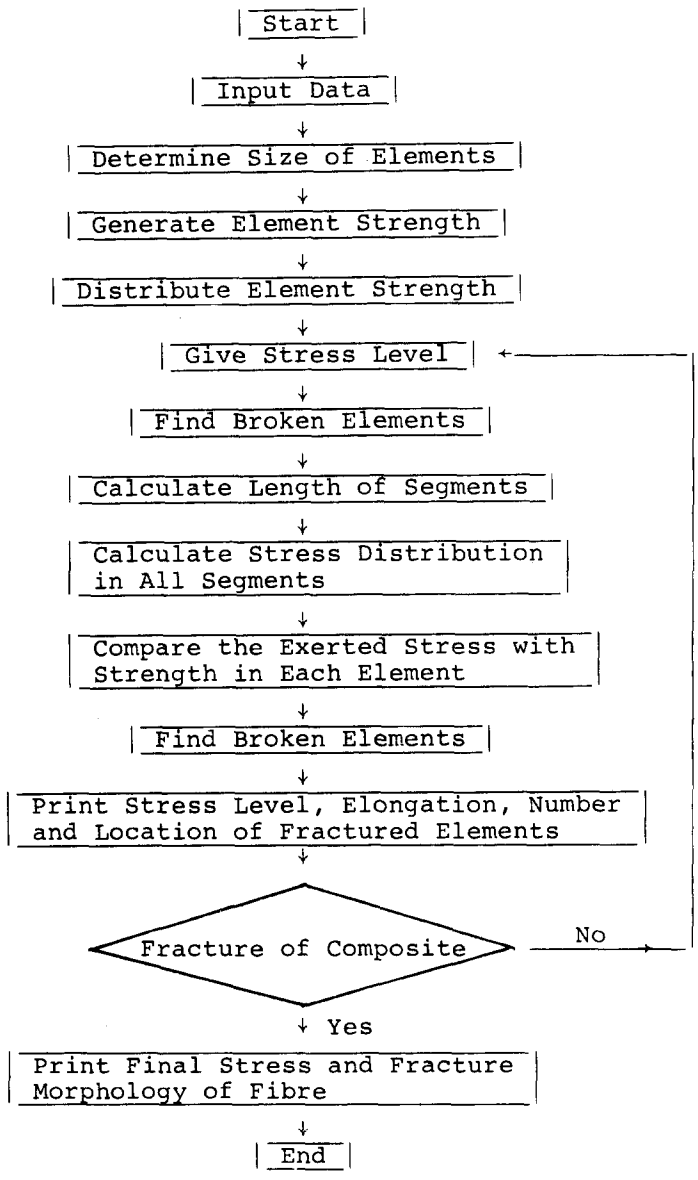

Figure 2 The flow chart of the present computer simulation.

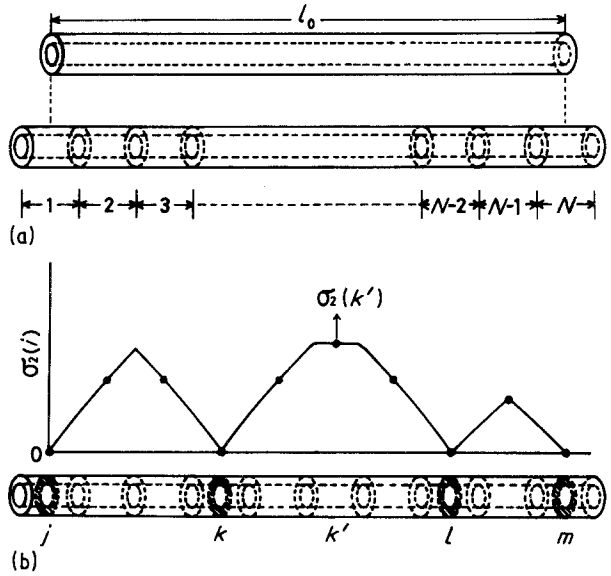

Figure 3 (a) Schematic representation for the determination of elements, and (b) the exerted tensile stress on the film of each element, where the j, k, l and mth elements have been broken already.

locations of $S(i) = 0$ were searched and the length of each segment was obtained. Substituting the applied stress and the length of the segment, together with the input values in (a) into the equations in the following paper [8], allowed the stress exerted in each element to be calculated.

(e) The exerted stress at the centre of each element was taken as the exerted stress on the element, to a first approximation. Noting the exerted stress at the centre of the ith element, $\sigma_2(i)$, we can determine whether the ith element can be broken or not by comparing $\sigma_2(i)$ with $S(i)$; if $\sigma_2(i)$ is higher than $S(i)$, the element is broken. When the ith element is broken, the $S(i)$ is said to be zero. Fig. 3b shows an example of stress distribution when the j, k, l and mth elements have been fractured (namely $S(j) = S(k) = S(l) = S(m) = 0$). If the exerted stress is higher than the strength, i.e. $S(k') \leqq \sigma_2(k')$, the k'th element is broken. Thus $S(k')$ becomes zero at this stress level.

(f) The elongation was calculated as follows. If the film is broken into p segments and the length of the qth element is l_q ($q = 1$ to p), the displacement at $x = l_q$ from $x = 0$ of the qth segment is given by $2U_1(x = l_q/2)$ where $U_1(x = l_q/2)$ is the displacement of the fibre at the centre of the qth segment. Therefore the total displacement of the composite from one to another end is given by $\Sigma_{q=1}^{p}\ 2U_1(x = l_q/2)$. As the initial length of the composite is l_0, the elongation e_c of the composite is given by

$$e_c = \left[\sum_{q=1}^{p} 2U_1(x = l_q/2)\right] \Big/ l_0 \qquad (2)$$

$U_1(l_q/2)$ was calculated using the calculation method presented in the following paper [8].

(g) At each stress level, the applied stress on the composite, the elongation and the number and location of fractured elements were printed out.

(h) The stress level was raised from zero to the fracture stress of the composite in steps of 0.1 MPa. At each stress level, the procedures of (d) to (g) were carried out. The fracture stress of the composite was given by the product of tensile strength of fibre and volume fraction of the fibre, since the coating film does not contribute to the strength of composite due to premature fracture.

3. Results of the computer simulation

3.1. Generated strength of coating film based on the Weibull distribution

The strength of the coated layer was assumed to obey the Weibull distribution as stated already. In general, the smaller the volume of the film, the stronger the film, since the film with a small volume has fewer defects. This is reflected in the Weibull distribution through the value of V in Equation 1. From Equation 1, the average strength of the film with a volume V, $S_{2,ave}$ is given by

$$S_{2,ave} = \sigma_0(1/V)^{1/m}\Gamma(1 + 1/m) \qquad (3)$$

where Γ is the gamma function and the coefficient of variation, CV, defined as the ratio of standard deviation to the average value, is given by

$$CV = \{\Gamma(1 + 2/m)/[\Gamma(1 + 1/m)]^2 - 1\}^{1/2} \qquad (4)$$

If one gives the values of $S_{2,ave}$ for a given V and CV, one can determine the values of σ_0 and m, using Equations 3 and 4. Thus the determined values of σ_0 and m are common for any value of V. Therefore, if one has the data of $S_{2,ave}$ and CV for only one value of V, one can know the distribution of strength for any value of V. Taking the case, where the average strength of the coating film $S_{2,ave}$ for $10^3\ \mu m^3$, defined as $S^0_{2,ave}$ in this work, is 1 GPa and the value of $CV = 10$ or 30%, hence the variations of $S_{2,ave}$ of the film coated on the fibre with a diameter of 1 mm as a function of l and c for a given value of $S^0_{2,ave}$ calculated from Equation 3, are shown in Fig. 4a and b, respectively. In the case of $S^0_{2,ave} = 1$ GPa, the values of σ_0 are 0.0265 GPa mm$^{(1/3.7)}$ and 0.330 GPa mm$^{(1/12)}$ and

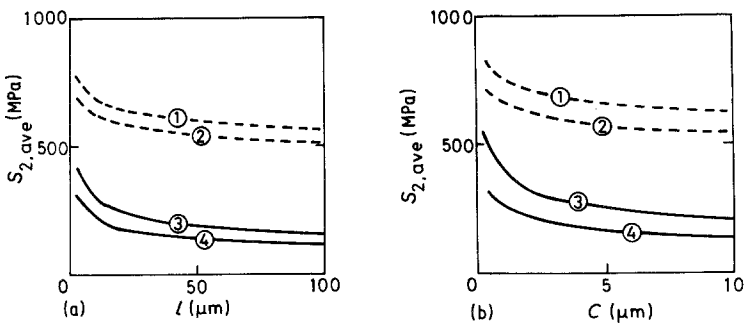

Figure 4 Variation of $S_{2,ave}$ of the film coated on the fibre with a diameter of 1 mm as (a) a function of l for (1) $c = 3\ \mu m$, $CV = 10\%$; (2) $C = 10\ \mu m$, $CV = 10\%$; (3) $c = 3\ \mu m$, $CV = 30\%$; (4) $c = 10\ \mu m$, $CV = 30\%$; and (b) as a function of c (1) $l = 10\ \mu m$, $CV = 10\%$; (2) $l = 50\ \mu m$, $CV = 10\%$; (3) $l = 10\ \mu m$, $CV = 30\%$; (4) $l = 50\ \mu m$, $CV = 30\%$; for a given value of $S^0_{2,ave} = 1$ GPa.

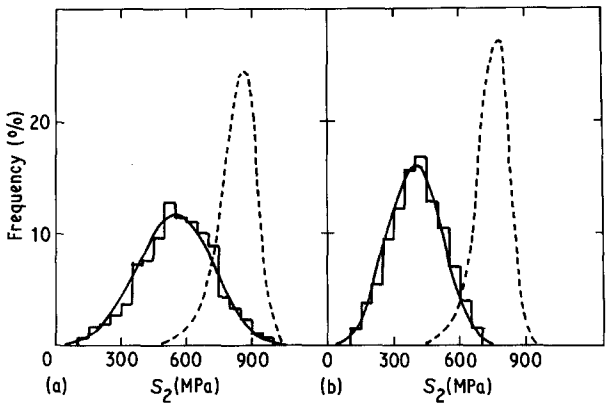

Figure 5 Distribution of strength of coating film with thickness (a) $c = 30\,\mu m$, (b) $c = 10\,\mu m$ of the fibre with a diameter of 1 mm for $S_{2,ave} = 1$ GPa for a given length of $l_e = 1\,\mu m$, together with histograms for $CV = 30\%$ generated by the computer. (——) $CV = 30\%$, (– – –) $CV = 10\%$.

those of m are 3.7 and 12 for $CV = 30$ and 10%, respectively. The curves in Fig. 4 reflect the feature of the Weibull distribution that $S_{2,ave}$ decreases with increasing l and c. According to the following paper [8], the tensile stress exerted on the segmented layer is high under tensile loading when the segment is long. Therefore it is suggested that long segments, having low strength but receiving high stress, tend to be fractured under loading.

Fig. 5 shows examples of distribution of the strength of coating film with the thicknesses of (a) $3\,\mu m$ and (b) $10\,\mu m$ on the fibre with a diameter of 1 mm for $CV = 10$ and 30% under a given gauge length of $1\,\mu m$ ($= l_e$ in the present simulation), together with the histograms for $CV = 30\%$ generated in the computer, where the $S^0_{2,ave}$ was taken to be 1 GPa. The distribution curves calculated by Equation 1 are well reproduced by the computer.

In the present work, computer simulation was carried out for various combinations of mechanical factors of E_1, E_2, G_1, G_2, σ_{1y}, ω and β, and geometrical factors of d, c and l_0, and statistical factors for strength of elements based on the Weibull distribution, m and σ_0. Among the factors, m and σ_0 were determined as stated above. τ_{1y} was taken to be $\sigma_{1y}/2$ and β to be $\omega E_1/4G_1$ as in the following paper [8]. The E_1, G_1 and l_0 were taken to be 100 GPa, 40 GPa and 1 mm, respectively. Other factors were varied as shown in Table I.

TABLE I Input values for the computer simulation

E_1	= 100 GPa
E_2	= 100 and 300 GPa
G_1	= 40 GPa
G_2	= 40 and 120 GPa
σ_{1y}	= 50, 100, 200 and 300 MPa
ω	= 0.001, 0.005 and 0.01
β	$= \omega E_1/4G_1$
d	= 0.5, 1, 2 and 4 mm
c	= 1, 3, 5, 7.5 and 10 μm
l_0	= 1 mm
l_e	= 1 μm
N	= 1001
CV	= 10(m = 12) and 30% (m = 3.7)
$S^0_{2,ave}$	= 0.5, 1, 2 and 4 GPa

3.2. Effects of thickness of coating film on multiple fracture of the film

Firstly in order to know the influence of thickness of coating film on multiple fracture of the layer, the value of c was changed for fixed values of $E_1 = 100$ GPa, $E_2 = 300$ GPa, $G_1 = 40$ GPa, $G_2 = 120$ GPa, $\sigma_{1y} = 300$ MPa, $\omega = 0.005$, $d = 1$ mm, $S^0_{2,ave} = 1$ GPa and $CV = 10$ and 30%. Fig. 6 shows a representative result of the computer simulation on the process of multiple fracture of the coating film. The solid lines show the location of fracture. It is clearly shown that the coating film is broken into more and more segments with increasing stress. The number of fractures of the coating film N_f increases and correspondingly the length of segments, l, decreases with increasing applied stress σ_c. As shown in Fig. 6, the long segments are fractured into short ones with increasing stress, but the fracture does not occur at the centre of them. Therefore the length of segments is widely scattered. Fig. 7 shows an example of the distribution of length of segments where the longitudinal axis shows the frequency. At low stresses, such as 280 MPa, the length is spread over a wide range, but at high stresses such as 400 MPa, as long segments have been fractured, the length of the segments are within a relatively narrow range of l values. It is interesting to note that the thinner coating film is fractured into shorter segments than the thicker one. This results from the difference of the exerted tensile stresses between the thinner and thicker films; i.e. the tensile stress exerted on the thinner film is higher than that on thicker one [8].

Fig. 8 shows variation of N_f with increasing σ_c for $c = 3$ and $10\,\mu m$. From the comparison of the curves shown in Fig. 8 to each other, the following features are found. (i) N_f is relatively small at low stress but suddenly increases at about $\sigma_c \approx 300$ MPa. This result can be explained by the fact that the exerted tensile stress on segments increases suddenly beyond the tensile yield stress of the fibre [8]. (ii) At high stresses far beyond the yield stress of the fibre, N_f remains nearly constant. This reflects the fact that the increasing rate of exerted tensile stress on segments of short length with increasing σ_c is so low at high stress levels [8] that the exerted tensile stress can merely exceed the strength of segments which have become short and therefore have a high strength as inferred from Fig. 4. (iii) The larger the CV, the larger becomes N_f. In the present simulation, the larger the CV, the lower becomes the strength of segments. This is reflected in this result. (iv) The thinner the layer, the more N_f becomes, as stated above.

Fig. 9 show the variation of length of segments at (a) 3% and (b) 10% elongations as a function of c. l increases with increasing c. It is interesting to point out that l increases parabolically with increasing c and it tends to increase linearly when CV is small. This dependency of l on c will be discussed in Section 3.9.

3.3. Effects of yield stress of fibre on multiple fracture of the film

The influence of yield stress of the fibre on multiple fracture of the coating film was studied by changing

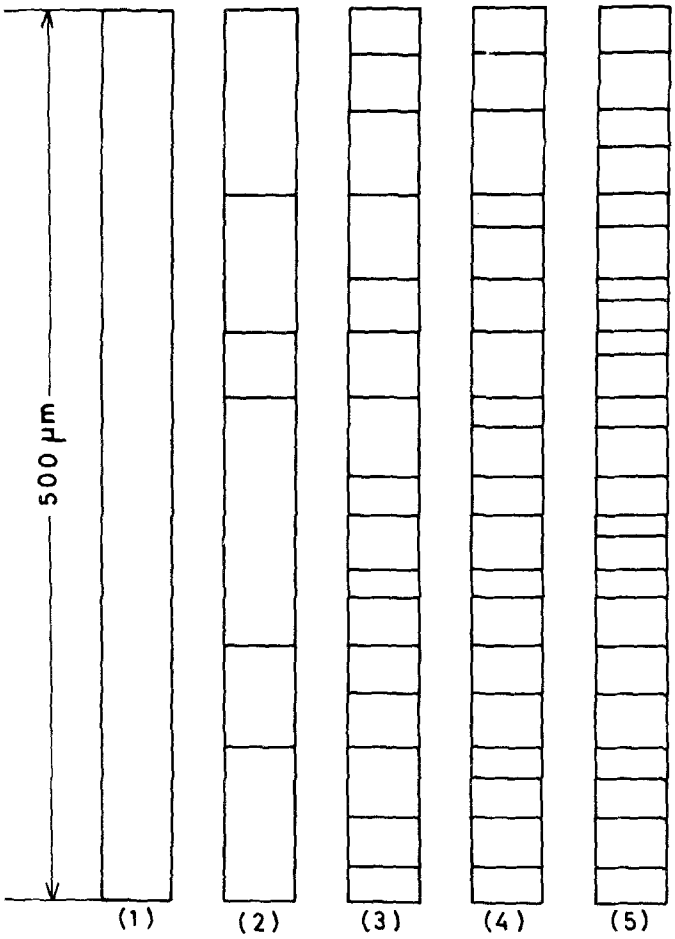

Figure 6 An example of multiple fracture of the coating film obtained by the computer simulation using the values of $E_1 = 100\,\text{GPa}$, $E_2 = 300\,\text{GPa}$, $G_1 = 40\,\text{GPa}$, $G_2 = 120\,\text{GPa}$, $\sigma_{1y} = 300\,\text{MPa}$, $\omega = 0.005$, $c = 10\,\mu\text{m}$, $d = 1\,\text{mm}$, $S^0_{2,\text{ave}} = 1\,\text{GPa}$ and $CV = 30\%$. (1) to (5) correspond to $\sigma_c = 50, 280, 305, 320$ and $400\,\text{MPa}$, respectively.

the value of σ_{1y} under fixed values of $E_1 = 100\,\text{GPa}$, $E_2 = 300\,\text{GPa}$, $G_1 = 40\,\text{GPa}$, $G_2 = 120\,\text{GPa}$, $\omega = 0.005$, $d = 1\,\text{mm}$, $c = 3$ and $10\,\mu\text{m}$, $CV = 30\%$ and $S^0_{2,\text{ave}} = 1\,\text{GPa}$. Fig. 10 shows the variation of N_f as a function of σ_c for $\sigma_{1y} = 50$, 100, 200 and 300 MPa. It is clearly seen that N_f increases gradually with increasing σ_c for $\sigma_c < \sigma_{1y}$ but rapidly at about $\sigma_c \sigma_{1y}$ and remains nearly constant at high stress level far beyond σ_{1y}. It is interesting that the higher the σ_{1y} value, the larger N_f becomes at high stress levels far beyond σ_{1y}. Fig. 11 shows the variation of l as a function of σ_{1y} at (a) $e_c = 3\%$ and (b) $e_c = 10\%$. l decreases with increasing σ_{1y}. Such a dependency of l on σ_{1y} has been shown previously [5].

3.4. Effects of diameter of fibre on multiple fracture of the film

The influence of diameter of fibre on multiple fracture of the film was studied by changing the value of d under fixed values of $E_1 = 100\,\text{GPa}$, $G_1 = 40\,\text{GPa}$, $E_2 = 300\,\text{GPa}$, $G_2 = 120\,\text{GPa}$, $\sigma_{1y} = 200\,\text{MPa}$, $\omega = 0.005$, $c = 10\,\mu\text{m}$, $CV = 10$ and 30% and

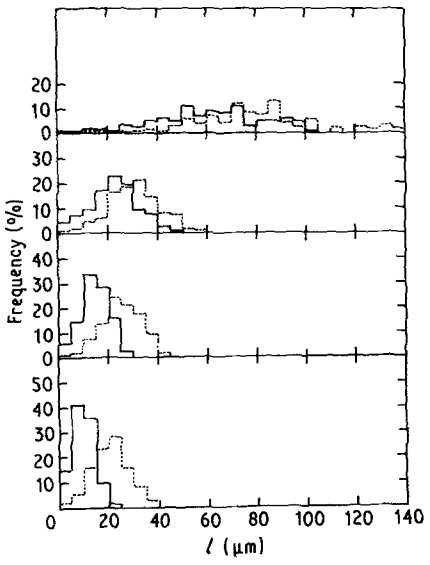

Figure 7 Distribution of the length of segments at (a) $\sigma_c = 280$, (b) $\sigma_c = 305$, (c) $\sigma_c = 320$ and (d) $\sigma_c = 400\,\text{MPa}$ for values of c: (——) $c = 3\,\mu\text{m}$, (– – –) $c = 10\,\mu\text{m}$. The values of the parameters other than c for the simulation are the same as those shown in the caption of Fig. 6.

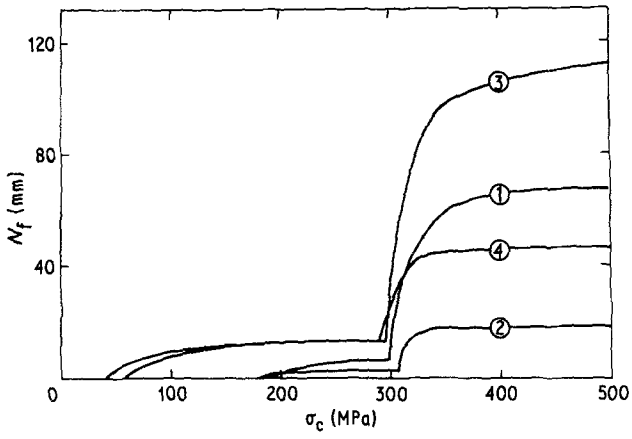

Figure 8 Variation of N_f with increasing σ_c. Input values: $E_1 = 100\,\text{GPa}$, $E_2 = 300\,\text{GPa}$, $G_1 = 40\,\text{GPa}$, $G_2 = 120\,\text{GPa}$, $\sigma_{1y} = 300\,\text{MPa}$, $\omega = 0.005$, $d = 1\,\text{mm}$, $S^0_{2,\text{ave}} = 1\,\text{GPa}$. (1) $CV = 10\%$, $c = 3\,\mu\text{m}$; (2) $CV = 10\%$, $c = 10\,\mu\text{m}$; (3) $CV = 30\%$, $c = 3\,\mu\text{m}$; (4) $CV = 30\%$, $c = 10\,\mu\text{m}$.

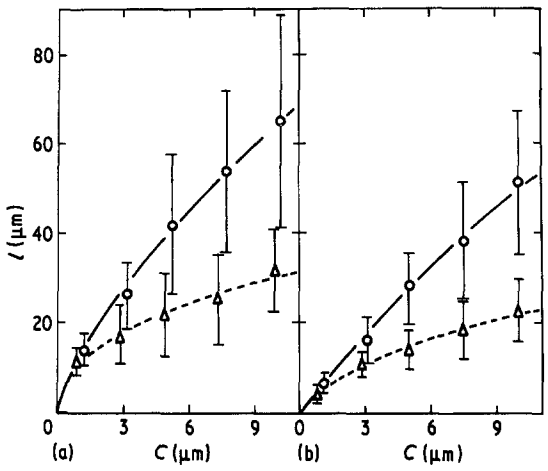

Figure 9 Variation of the length of segments as (a) e_c = 3% and (b) e_c = 10% elongation as a function of c. Input values: same as those shown in the caption of Fig. 8. (○) CV = 10%, (△) CV = 30%.

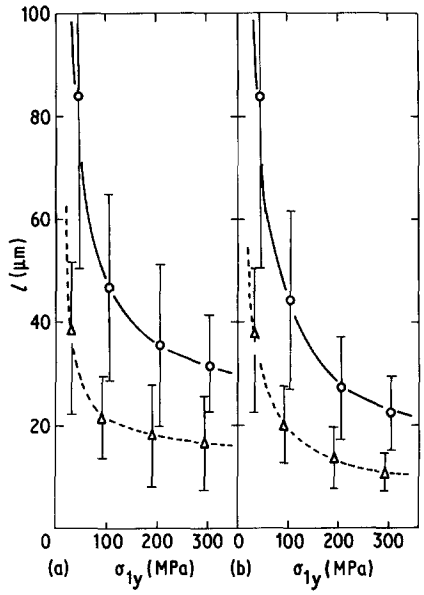

Figure 11 Variation of the length of segments at (a) e_c = 3% and (b) e_c = 10% elongations as a function of σ_{1y}. Input values: same as those shown in the caption of Fig. 10. (△) c = 3 μm; (○) c = 10 μm.

$S^0_{2,ave}$ = 1 GPa. Fig. 12 shows the example of the variation of N_f as a function of σ_c. It is evident that N_f increases with increasing d. This results from the following two reasons. (i) The larger the d, the higher becomes the exerted tensile stress on segments [8]. (ii) The volume of segments on thicker fibre is larger than that on the thinner one for a given length. Therefore the segments on the thicker fibre are weaker than those on the thinner fibre as known from Equations 1 and 3. Fig. 13 shows the variation of l as a function of d at 3 and 10% elongation. The dependency of l on d for small CV is weaker than that for large CV. This difference will be discussed in Section 3.9.

3.5. Effects of strength of coating film on multiple fracture of the film

The influence of strength of the coating film on multiple fracture of the film was studied by changing the value of $S^0_{2,ave}$ from 0.5 to 4 GPa under the fixed values of E_1 = 100 GPa, G_1 = 40 GPa, E_2 = 300 GPa, G_2 = 150 GPa, σ_{1y} = 200 MPa, ω = 0.005, c = 3 μm and CV = 10 and 30%. Fig. 14 shows examples of the variation of N_f as a function of σ_c. As expected, the stronger the film, the smaller becomes N_f. Fig. 15 shows the variation of l as a function of $S^0_{2,ave}$ at 3 and 10% elongation. There is a feature that the dependency of l on $S^0_{2,ave}$ for small CV is weaker than that for large CV.

3.6. Effects of Young's modulus of coating film on multiple fracture of the film

The influence of Young's modulus of the coating film on multiple fracture of the film was studied by changing the value of E_2 under fixed values of E_1 = 100 GPa, G_1 = 40 GPa, σ_{1y} = 200 MPa, ω = 0.005, d = 1 mm, c = 3 and 10 μm, CV = 30% and $S^0_{2,ave}$ = 1 GPa. Fig. 16 shows the variation of N_f as a function of σ_c for E_2 = 100 and 300 GPa. In this simulation, the values of G_2 corresponding to 100 and 300 GPa were taken to be 40 an 120 GPa from the relation of $G_2 = E_2/[2(1 + \nu_2)]$ where ν_2 is the

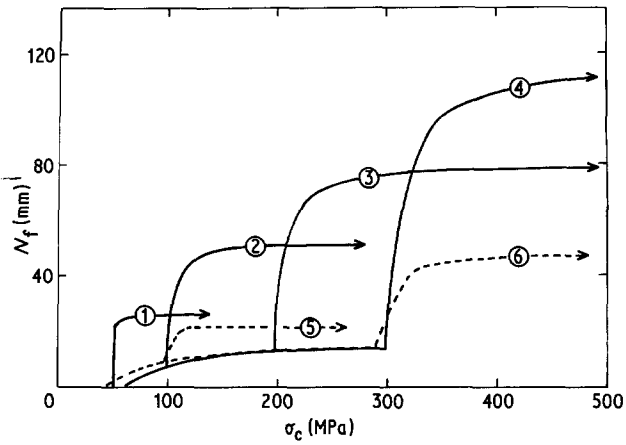

Figure 10 Variation of N_f with increasing σ_c. Input values: E_1 = 100 GPa, E_2 = 300 GPa, G_1 = 40 GPa, G_2 = 120 GPa, ω = 0.005, d = 1 mm, $S^0_{2,ave}$ = 1 GPa and CV = 30%. (1) σ_{1y} = 50 MPa, c = 3 μm; (2) σ_{1y} = 100 MPa, c = 3 μm; (3) σ_{1y} = 200 MPa, c = 3 μm; (4) σ_{1y} = 300 MPa, c = 3 μm; (5) σ_{1y} = 100 MPa, c = 10 μm; (6) σ_{1y} = 300 MPa, c = 10 μm.

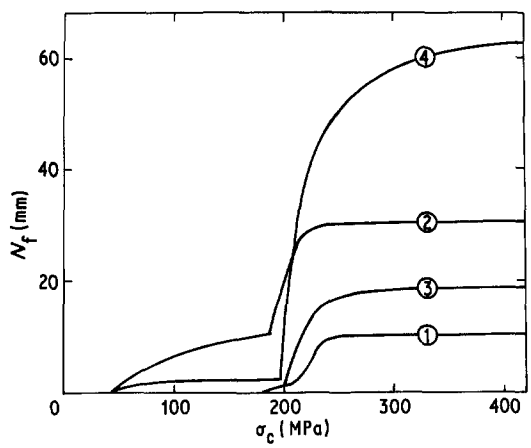

Figure 12 Variation of N_f with increasing σ_c. Input values: E_1 = 100 GPa, E_2 = 300 GPa, G_1 = 40 GPa, G_2 = 120 GPa, σ_{1y} = 200 MPa, ω = 0.005, d = 1 mm, c = 10 μm, $S^0_{2,ave}$ = 1 GPa. (1) d = 0.5 mm, CV = 10%; (2) d = 0.5 mm, CV = 30%; (3) d = 5.0 mm, CV = 10%; (4) d = 5.0 mm, CV = 30%.

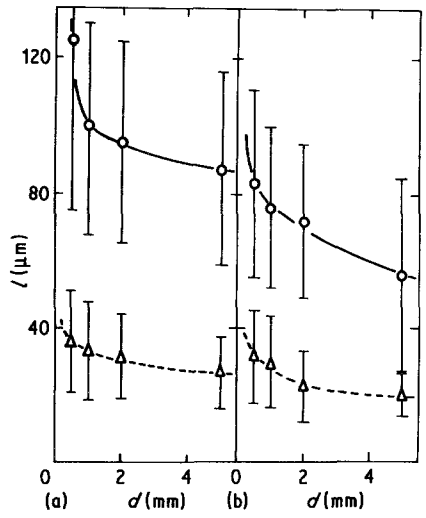

Figure 13 Variation of the length of segments at (a) e_c = 3% and (b) e_c = 10% elongation as a function of d. Input values: same as those shown in the caption of Fig. 12. (○) CV = 10%; (△) CV = 30%.

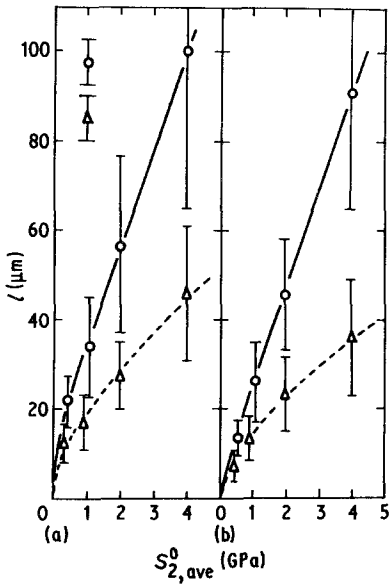

Figure 15 Variation of the length of segments at (a) e_c = 3% and (b) e_c = 10% elongation as a function of $s^0_{2,ave}$. Input values: same as those shown in the caption of Fig. 14. (○) CV = 10% (△) CV = 30%.

Poisson's ratio, taken to be 0.25. The dependency of N_f on E_2 is very weak.

The dependency of N_f on ω was also studied by changing ω from 0.001 to 0.01. The results of the simulation showed that the dependency is very weak as is the dependency on E_2.

3.7. Elongation to failure of composite specimens

Noting the elongation to failure of the fibre as e_{fu}, the composite specimens fail when the elongation of the cross-section, where the film has fractured, exceeds e_{fu}. In other words, the composite specimens fail when the stress on the fibre at this cross-section exceeds the tensile strength of the fibre. The elongation to failure of the composite specimens, e_{cu}, is lower than e_{fu} since, as the load borne by the composites is the same at any cross-section, the film supports the applied load in cross-sections other than those where the film has fractured. The variation of e_{cu} as a function of (a) c, (b) σ_{1y}, (c) d and (d) $S^0_{2,ave}$ for the cases of e_{fu} = 10 and 20% is shown in Fig. 17 where the input data for (a) to (d) are the same as those stated in sections 3.2, 3.3, 3.4 and 3.5, respectively. The results shown in Fig. 17 show the following features. (i) The thicker the film, the lower becomes e_{cu}. (ii) The higher the yield stress of fibre, the lower becomes e_{cu}. (iii) The thicker the diameter of the fibre, the higher becomes e_{cu}. (iv) The higher the strength of the film; namely the higher the $S^0_{2,ave}$ and the lower the CV, the lower becomes e_{cu}.

3.8. The increase in fibre stress due to coating

As the coating film fractures continually, the fibre should deform more in the cross-sections where the film is fractured than in the sections where the film is not fractured. This effect gives an increase in fibre stress in comparison with the stress on the uncoated fibre at a given elongation. Fig. 18 shows some examples of σ_1–e_c curves. In the range investigated in this work, the σ_1 for coated fibre was higher than that

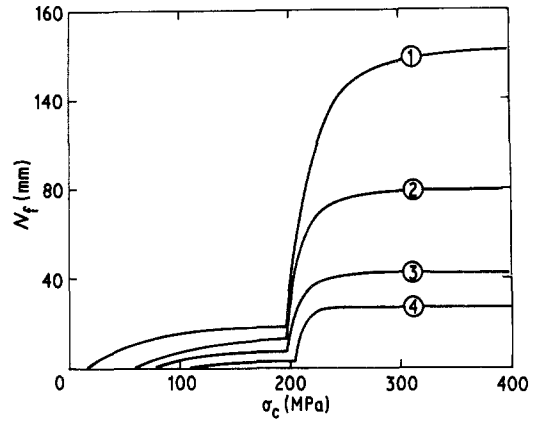

Figure 14 Variation of N_f with increasing σ_c. Input values: E_1 = 100 GPa, E_2 = 300 GPa, G_1 = 40 GPa, G_2 = 120 GPa, σ_{1y} = 200 MPa, ω = 0.005, d = 1 mm, c = 3 μm, and CV = 30%. (1) $S^0_{2,ave}$ = 0.5 GPa; (2) $S^0_{2,ave}$ = 1.0 GPa; (3) $S^0_{2,ave}$ = 2.0 GPa; (4) $S^0_{2,ave}$ = 4.0 GPa.

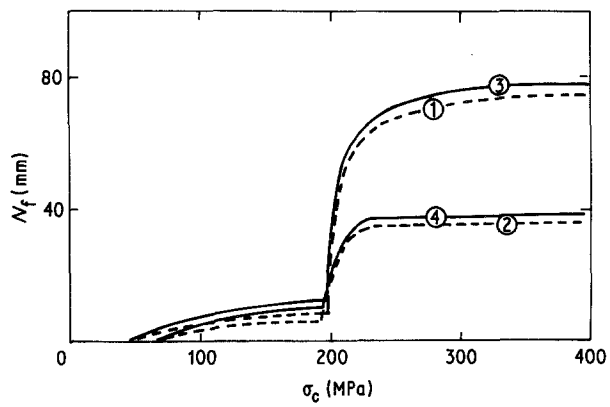

Figure 16 Variation of N_f with increasing σ_c. Input values: E_1 = 100 GPa, G_1 = 40 GPa, σ_{1y} = 200 MPa, ω = 0.005, d = 1 mm, CV = 30% and $S^0_{2,ave}$ = 1 GPa. (1) E_2 = 100 GPa, c = 3 μm; (2) E_2 = 100 GPa, c = 10 μm; (3) E_2 = 300 GPa, c = 3 μm; (4) E_2 = 300 GPa, c = 10 μm.

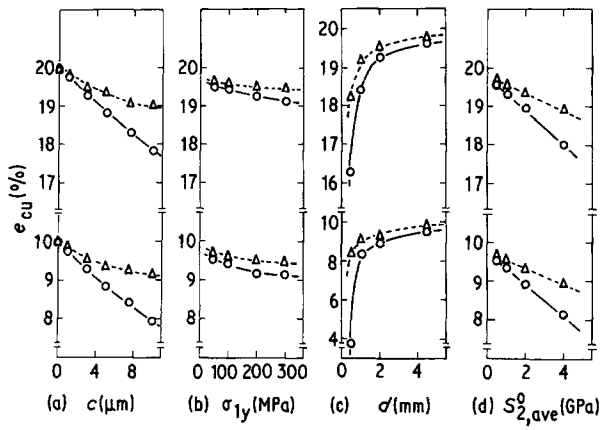

Figure 17 Variation of e_{cu} as a function of (a) c: (○) CV = 10%, (△) CV = 30%; (b) σ_{1y}: (○) c = 10 μm, (△) c = 3 μm; (c) d: (○) CV = 10%, (△) CV = 30%; and (d) $S^0_{2,ave}$: (○) CV = 10%, (△) CV = 30% for e_{fu} = 10 and 20%. The input values for (a) to (d) are the same as those shown in the captions of Figs 8, 10, 12 and 14, respectively.

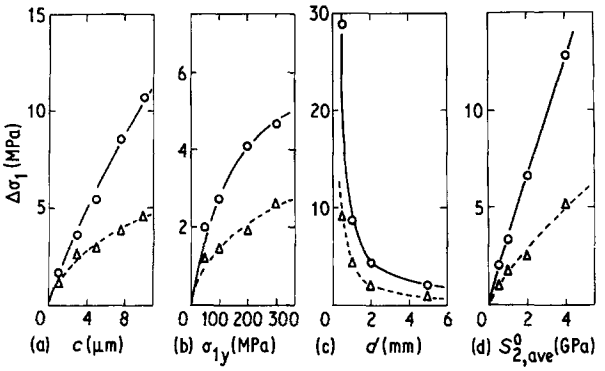

Figure 19 Difference of tensile stress between coated and uncoated fibres at 3% elongation as a function of (a) c: (○) CV = 10%, (△) CV = 30%; (b) σ_{1y}: (○) c = 10 μm, (△) c = 3 μm; (c) d: (○) CV = 10%, (△) CV = 30%; and (d) $S^0_{2,ave}$: (○) CV = 10%, (△) CV = 30%. Input values for (a) to (d) are the same as those shown in the captions of Figs 8, 10, 12 and 14.

for uncoated fibre. Fig. 19 shows some examples of the difference in fibre stress $\Delta\sigma_1$ between coated and uncoated fibres at 3% elongation. The input data for (a) to (d) in Fig. 19 were the same as those stated in sections 3.2, 3.3, 3.4 and 3.5, respectively. $\Delta\sigma_1$ is high when values of c, σ_{1y} and $S^0_{2,ave}$ are large and when the value of d is small. The dependency of $\Delta\sigma_1$ on these parameters is just the reverse of the dependency of e_{cu} on them.

The fact, that the fibre is strengthened by the coating although the coating material is fractured and supports no load at the cross-section where the coating material is fractured, has been observed [1, 2, 5]. To account for this fact, radial and tangental stresses in fibre and coating film should be taken into consideration [2]. In this respect the present result is not rigid enough to explain the strengthening effect, since the radial and tangental stresses are neglected in the calculation [8]. However, as these stresses are not high at low elongations yet becoming very high at high elongations [2], the strengthening effect at low elongations could be described to some extent in the present simulation.

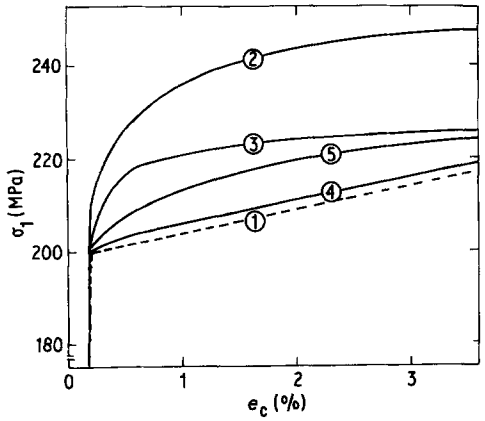

Figure 18 Tensile stress of fibre σ_1 as a function of e_c for some examples. Input values: E_1 = 100 GPa, E_2 = 300 GPa, G_1 = 40 GPa, G_2 = 120 GPa, σ_{1y} = 200 MPa, ω = 0.005, c = 10 μm, $S^0_{2,ave}$ = 1 GPa. (1) uncoated; (2) d = 0.5 mm, CV = 10%; (3) d = 1 mm, CV = 10%; (4) d = 5 mm, CV = 10%; (5) d = 0.5 mm, CV = 30%.

3.9. Comparison of the results of the present simulation with those predicted by the modified Kelly–Tyson model

Modifying the Kelly–Tyson model [7], the condition for the segments with average length l_{ave} and average strength $S_{2,ave}$ to be broken is, is given by

$$\pi d\tau_{i,ave} l_{ave}/2 = \pi c d S_{2,ave} \quad (5)$$

as c is small compared to d in the present work. $\tau_{i,ave}$ is usually taken to be τ_{1y}. This value is not so much different from the value calculated by the method in [8] in the present work. The difference is less than 20% at 10% elongation. The $S_{2,ave}$ in Equation 5 is given by Equation 3. Combining Equations 3 and 5 and setting $c \ll d$ and $\tau_{i,ave} = \tau_{1y} = \sigma_{1y}/2$, we have

$$l_{ave} = \{[4\sigma_0\Gamma(1 + 1/m)]^m/\pi\}^{[1/(m+1)]} d^{[-1/(m+1)]} \times c^{[(m-1)/(m+1)]} \sigma_{1y}^{[-m/(m+1)]} \quad (6)$$

Equation 6 gives a simple expression of l_{ave}, being very convenient for applications. However, one should be careful on the application of Equation 6 in the following points. (i) Equation 6 lacks statistical treatment of strength and location of fracture of the segments, since it is assumed that all the segments have the same length and the same strength, and the location of fracture is always the centre of the segments. (ii) Although $\tau_{i,ave}$ is a function of stress level or elongation, it is taken as τ_{1y}, as stated already. (iii) Equation 6 does not include the term of stress level or elongation. The range of stress level where Equation 6 can be applied is not clear. (iv) Equation 6 assumes that the fibre is plastic in shear in the whole range of l_{ave}. However, such a situation is not always found, especially when the stress level is not high even if the fibre shows plastic deformation in tension in the whole range of l_{ave} [8]. (v) According to the following paper [8], when the fibre becomes plastic in the whole range of l_{ave} at high stress levels, the dependency of the exerted tensile stress in segments on σ_c becomes weak. Under this condition, the segments hardly fracture and the length of segments does not vary as known from the present simulation. This suggests that Equation 6 can be applied only in the later stages of

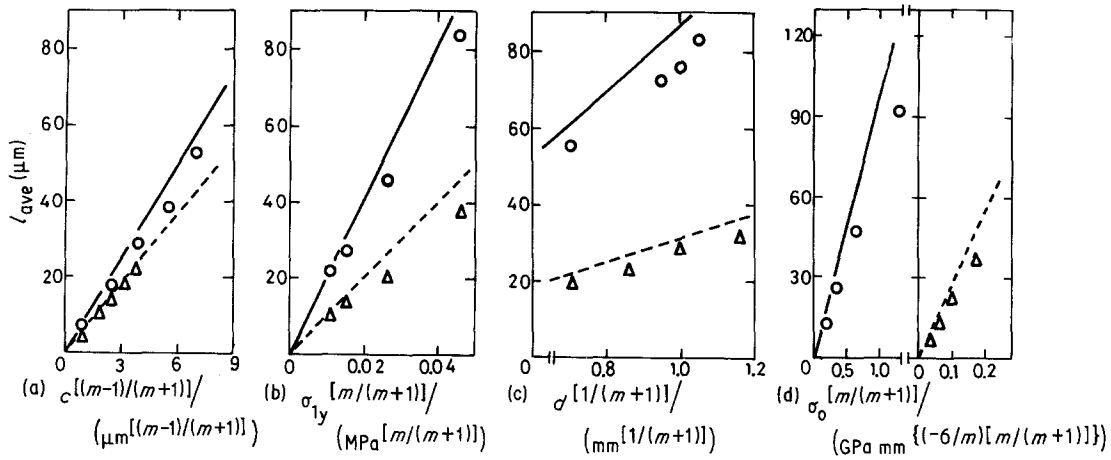

Figure 20 Comparison of l_{ave} at 10% elongation obtained by the present simulation with that predicted by Equation 6. The data obtained by the simulation in Figs. 9b, 11b, 13b and 15b are plotted against (a) $c^{[(m-1)/(m+1)]}$: (○) Sim, CV = 10%; (——) Cal, CV = 10%; (△) Sim CV = 30%); (— — —) Cal, CV = 30%. (b) $\sigma_{1y}^{[m/(m+1)]}$: (○) Sim, c = 10 μm; (——) Cal, c = 10 μm; (△) Sim, c = 30 μm; (— — —) Cal, c = 30 μm. (c) $d^{[1/(m+1)]}$: (○) Sim, CV = 10%; (——) Cal, CV = 10%; (△) Sim, CV = 30%; (— — —) Cal, CV = 30%. (d) $\sigma_0^{[m/(m+1)]}$: (○) Sim, CV = 10%; (——) Cal, CV = 10%; (△) Sim, CV = 30%; (– – –) Cal, CV = 30%.

deformation where the segments hardly fracture to a first approximation.

As stated above, Equation 6 can be applied when l_{ave} remains nearly constant at high stress levels or elongations. In the present work, the values of l_{ave} at 10% elongation obtained by the computer simulation were compared with those predicted by Equation 6. Fig. 20 shows the results of the comparison where the data shown in (a) to (d) were taken from Figs 9b, 11b, 13b and 15b. It is surprising that Equation 6 agrees fairly well the results of the simulation, although it is derived roughly. This result indicates that the Kelly–Tyson model is very useful to roughly describe the multiple fracture behaviour of the coating film at high elongations. Also the results of the simulation that l_{ave} is not so much affected by E_2 and ω can be understood from Equation 6, since Equation 6 has no term of E_2 and ω. Thus without making efforts to carry out a computer simulation, one can directly deduce the behaviour of the film at high elongations from Equation 6. Of course, when one wants to know not only the average length but also the distribution of length of segments or to know the increase in fibre stress due to the coating and so on in the whole range of deformation more precisely, one cannot employ Equation 6. For such a case, the computer simulation technique is helpful as shown in this work.

4. Conclusions

Multiple fracture phenomenon of coating films on ductile metal fibre (or wire) was studied by means of a computer simulation technique. For various combinations of mechanical and geometrical factors, the simulation was carried out. Main results are summarized as follows.

1. The thinner the coating film, the higher the yield stress of the fibre, the thicker the fibre and the lower the strength of the film, the larger becomes the number of fracture of the film and the shorter becomes the length of segments. The Young's modulus of the coating film and strain hardening coefficient of the fibre does not affect so much the number of fractures of the film within the range investigated.

2. The thicker the film, the higher the yield stress of the fibre, the thinner the fibre and the lower the strength of the film, the lower becomes the elongation to failure.

3. The increase in fibre stress due to coating becomes high when the film becomes thick, the yield stress of the fibre becomes high, the diameter of the fibre becomes thin and the strength of the film becomes high.

4. The Kelly–Tyson model is found to be a useful tool to describe multiple fracture behaviour of the film for the deformation stage where the film becomes segmented at high elongations.

References

1. J. S. THORNTON and A. D. THOMAS Jr, *Metall. Trans.* **3** (1972) 637.
2. S. OCHIAI and Y. MURAKAMI, *Met. Sci.* **10** (1976) 401.
3. I. PFEIFFER and E. SPRINGER, *Z. Metallkunde* **63** (1977) 667.
4. S. NOURBAKHSH, Y. S. HASCICEK, M. J. GORINGE and J. W. MARTIN, *J. Mater. Sci.* **17** (1982) 3204.
5. T. SHIKATA, H. SHINNO, M. FUKUTOMI, M. FUJITSUKA and M. OKADA, *ibid.* **18** (1983) 3092.
6. *Idem, ibid.* **18** (1983) 3099.
7. A. KELLY and W. R. TYSON, *J. Mech. Phys. Solids* **13** (1965) 329.
8. S. OCHIAI and K. OSAMURA, *J. Mater. Sci.* **21** (1986) 2744.
9. W. WEIBULL, *J. Appl. Mech.* **18** (1951) 293.

Received 30 September
and accepted 4 October 1985